Investigation of Hydrogen-Bonding Mediated Molecular Packing of Diketopyrrolopyrrole based Donor-Acceptor Oligomers in the Solid State

Kun Yang,[1†] Xiang Li,[1†] Yi-Fan Huang,[2] Ram S. Bhatta,[1] Jiawei Liu,[1] Mesfin Tsige,[1] Chien-Lung Wang[2], Stephen Z. D. Cheng[1] and Yu Zhu[1]*

[1]Department of Polymer Science, College of Polymer Science and Polymer Engineering, The University of Akron, 170 University Circle, Akron, Ohio 44325-3909, United States

[2]Department of Applied Chemistry, National Chiao Tung University, 1001 Ta Hsueh Road, Hsinchu 30010, Taiwan

E-mail: yu.zhu@uakron.edu

Abstract Two diketopyrrolopyrrole (DPP)-based Donor-Acceptor oligomers with thermal labile 2-methylhexyl-2-oxylcarbonyl (mHoc) groups, mHocPBT and mHocTBT, were synthesized and characterized to study the hydrogen-bonding mediated molecular packing in solid state. The soluble oligomers can be converted to strong intermolecular hydrogen-bonded and pigment-like materials HPBT and HTBT by annealing the casted solid film at a temperature between 180 and 200 °C. The formation of intermolecular hydrogen bonding significantly altered the conformation of the molecules, molecular packing structure and related optical properties of the oligomers, with HPBT molecule exhibiting bathochromic shift and HTBT molecule exhibiting hypsochromic shift on UV/Vis spectra. Spin-casted mHocTBT and HTBT films also exhibited interesting morphology and charge transport properties. Even though the single mHocTBT oligomer molecule has a better

coplanar molecular conformation as compared with that of HTBT, an enhanced π-π stacking structure and larger crystal grain size rendered HTBT film better charge transport performance.

Keywords

Conjugated Molecules, Hydrogen Bond, Molecular Packing

Introduction

Solution-processable organic molecular and polymeric semiconductors have drawn much attentions over the past two decades [1-5]. Due to their possibilities in fabricating low-cost, flexible, printable and even wearable electronics [6], organic semiconductors have been widely studied as the active materials for organic light-emitting diodes (OLEDs) [7], organic photovoltaics (OPVs) [8,9] and organic field-effect transistors (OFETs) [10,11]. Compared to the inorganic counterparts, organic π-conjugated semiconductors offer many key advantages. For example, the molecular structure of conjugated small molecules and polymers can be tailored through sophisticated molecular design. By the incorporation of different functionality, their physical and chemical properties can be accurately modulated [12,13]. Additionally, the solution-based low temperature processing of materials affords the compatibility of device fabrication with plastic substrates as well as the high through-put printing techniques. This allows the production of large-area, low-cost and flexible electronic devices. Although various benefits are promised, for OFETs applications, organic semiconductors still suffer from their low charge mobility when compared to the silicon-based materials. One of the greatest challenges in organic semiconductors is to control the assembly of organic molecules, which have relatively weak intermolecular interactions in their solid states [14]. Among the organic materials used for OFETs, conjugated small molecules represent one important subset due to their easy purification process, specified molecular weight, and better control for molecular structures [11]. Highly crystalline films required for efficient

charge transport can be achieved with conjugated small molecules [15]. Therefore, a tremendous amount of conjugated small-molecule-based FET devices have been fabricated [16-20], giving increasing charge mobilities that are already comparable to amorphous silicon [15,21,22]. Among these miscellaneous structures, especially organic pigment-derived small molecules and oligomers [23-32], diketopyrrolopyrrole (DPP)-based conjugated small molecules represent one class of the most extensively studied FET materials due to the remarkable properties of DPP moieties [33-40]. The rigid bicyclic structure of DPP cores endows the molecules an excellent backbone coplanarity and enhances efficient π-conjugation. The strong electron-withdrawing nature of DPP facilitates the intramolecular charge transfer (ICT) process when it is coupled with an electron donor unit (thiophene, phenyl rings, etc.) to form a donor-acceptor (D-A) type material. Most importantly, the strong interchain donor-acceptor interactions of the DPP-based D-A molecules can give a decreased π-π stacking distance and strengthen molecular self-assembly capability. As mentioned above, the weak intermolecular interaction in organic semiconductor materials is usually responsible for the disordered molecular alignment and poor device performance. Introducing stronger intermolecular interactions between the discrete molecules, such as hydrogen bonding, is an efficient strategy to improve the molecular connections and facilitate charge transport of materials in the solid state [41-54]. In this work, two DPP-based D-A type oligophenylenethiophene molecules with latent hydrogen-bonding networks were reported. With those latent hydrogen-bonding units, the molecules are solution processable and can generate actual intermolecular hydrogen bonding network after the labile groups are removed by thermal annealing of the casted solid film. The structure and properties of *in-situ* generated hydrogen-bonded DPP D-A oligomers were investigated.

Results and discussion

Synthesis of Materials

Previous research from our group and others used *tert*-butyloxyl carbonyl (*t*-Boc) group as removable side chains blocking the hydrogen-bonding donor site [42,49,55,56]. However, the relatively short chain length of t-Boc group can only provide limited solubility for small pigment molecules, which is not enough for longer oligomers and polymers. For this reason, a new thermal labile group with stronger solubilizing ability, 2-methylhexyl-2-oxylcarbonyl (mHoc), was introduced to the DPP core of the designed oligomer molecules, mHocPBT and mHocTBT (Scheme 1). Then a bithiophene moiety was coupled to the DPP core with different inner substituted aromatic rings via Stille coupling. Stille coupling is chosen due to its mild reaction condition, which allows the use of mHoc-Boc group. Similar Suzuki coupling is also available, but it should be carried out under micellar/emulsion conditions. [57] By using the mHoc group, both oligomers can be readily dissolved in common organic solvents for the solution-processing based OFET device fabrication. After the devices fabrication, the mHoc group can be easily removed, triggering the formation of intermolecular hydrogen-bonding systems in the active layer of the devices.

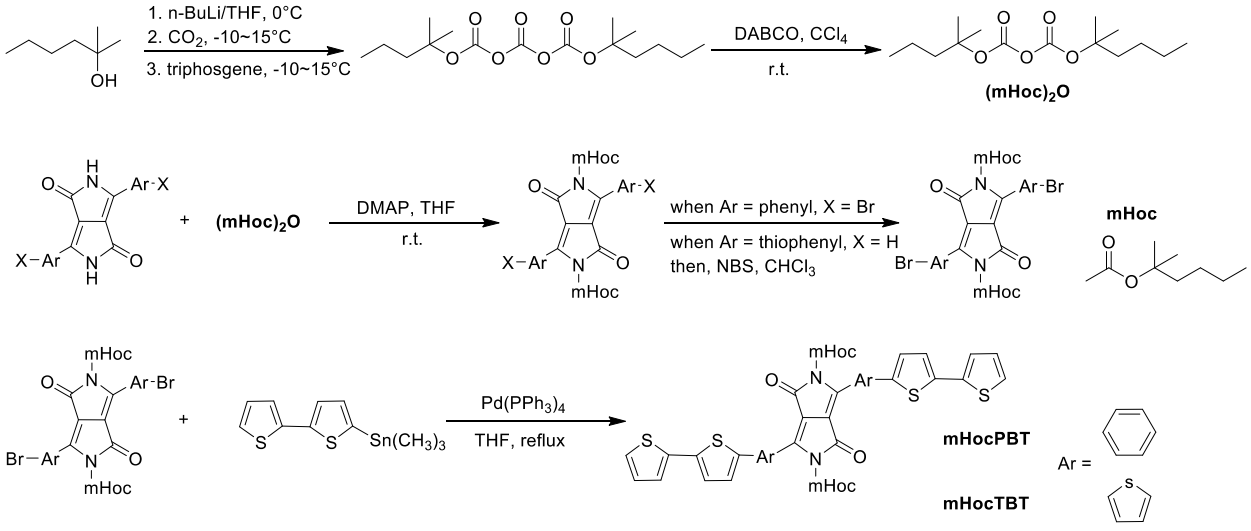

Scheme 1. Synthesis scheme of mHocPBT and mHocTBT molecules. Thermal treatment can remove mHoc side groups on the oligomers to generate actually hydrogen bonded networks. The molecules are noted as HPBT and HTBT respectively after removal of side groups.

The structure and synthetic route of mHocPBT and mHocTBT molecules were illustrated in Scheme 1 and Figure S1 (SI). Similar to the strategy used to synthesize the various *tert*-butoxycarbonyl (*t*-Boc) functionalized latent pigments in literatures [42,49,58,59], a dicarbonate compound (di-(2-methylhexan-2-yl-oxycarbonyl dicarbonate, $(mHoc)_2O$) was first synthesized following the reported method [60]. The DPP pigments were treated with $(mHoc)_2O$ in the existence of 4-(dimethylamino)pyridine (DMAP).The resulting mHoc-substituted molecules exhibited excellent solubility and were used in the following coupling reactions, affording the final mHocPBT and mHocTBT D-A oligomers. Both mHocPBT and mHocTBT molecules exhibited good solubility (> 5 mg/ml) in common organic solvents such as $CHCl_3$, toluene and THF, allowing the solution processed device fabrication. In comparison, two similar oligomers, *t*-BocPBT and *t*-BocTBT, in which the mHoc group was replaced with a shorter *t*-Boc group, only showed limited solubility (< 1 mg/mL in $CHCl_3$, THF and toluene), rendering it difficult for solution-processing technique such as spin-coating.

The thermal behavior of mHocPBT and mHocTBT molecules was firstly studied by thermogravimetric analysis (TGA). As shown in Figure 1a, the TGA curves of both mHocPBT and mHocTBT confirm the occurrence of the thermolysis reactions at 150~200 °C. The mass loss is approximately 31% to 33%, which corresponds well to the decomposition of mHoc groups and formation of hydrogen-bonding site-containing lactam group. Previous results have proved the decomposition of mHoc group generates gaseous CO_2 and 2-methyl-2-hexene (boiling point 91°C)

[61], indicating the complete cleavage. Further temperature increase doesn't cause any structure decomposition until 400 °C. This proves the excellent thermal stability of the conjugated DPP-thiophene backbone (i.e. HPBT and HTBT molecules) after the side chain removal. For comparison, TGA analysis of *t*-BocPBT and *t*-BocTBT was also carried out (Figure S2). Similar thermal stability of mHoc and *t*-Boc group functionalized PBT and TBT molecules can be observed. The initial decomposition temperature data and weight loss percentage of these molecules were summarized in Table S1.

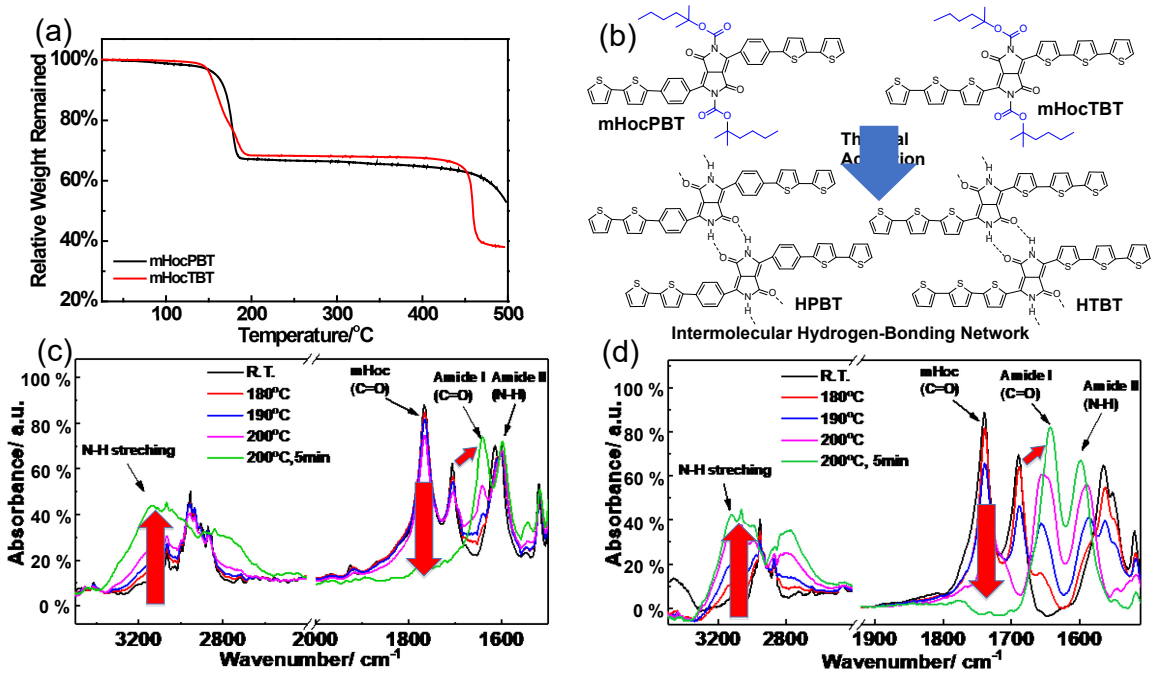

Figure 1. (a) TGA curves of mHocPBT (black) and mHocTBT (red) oligomers. (b) Scheme of mHoc group cleavage and formation of intermolecular hydrogen bonding. (c), (d) Kinetic FT-IR spectra of mHocPBT (c) and mHocTBT (d) molecules at gradually increased temperatures.

With the thermal deprotection of mHoc groups, the activation of the H-Bonding between the oligomers were expected (Figure 1b), which was further validated by Fourier transform infrared (FT-IR) spectroscopy. The detailed kinetic evolution of the functional groups in the mHocPBT

and mHocTBT molecules under elevated temperature was monitored and shown in Figure 1c and 1d. As shown in Figure 1c, the characteristic stretching vibration band of the carbonyl group (C=O from mHoc group) at 1765 cm^{-1} gradually diminished and finally disappeared upon annealing, indicating the successful removal of the mHoc protective group in the mHocPBT molecules. A new broad absorption peak between 2600 cm^{-1} and 3500 cm^{-1} appeared in the high wavenumber region, which can be attributed to the hydrogen-bonded N-H stretching vibration mode in the deprotection-generated lactam (H-N-C=O) group [42]. The formation of amide with a secondary amine can be also confirmed by the presence of absorption bands at 1641 cm^{-1} (amide I band, C=O stretching) and 1600 cm^{-1} (amide II band, N-H bending) [62]. The shift of carbonyl group stretching on the DPP core from 1706 cm^{-1} to 1641cm^{-1} with lower energies was conducive to formation of intermolecular hydrogen bonding at the corresponding carbonyl groups. Similar transition was observed in the anneal process of mHocTBT molecules as shown in Figure 1(d). These data provided strong evidence of the triggering of intermolecular hydrogen-bonding networks in the thermally annealed DPP D-A oligomers.

Photophysical and Electrochemical Properties

The optical properties of the oligomers were studied by UV/Vis spectroscopy. As shown in Figure S3, the D-A oligomers significantly shifted the maximum absorption peak of the DPP chromophores to the long wavelength range. The corresponding bathochromic shifts for mHocPBT and mHocTBT were 54 nm and 80 nm (in THF solvent), respectively. To fully understand the side chain's impact to the optical properties of the oligomers, the UV/Vis spectra of oligomers mHocPBT and mHocTBT in solution (DMF and THF as solvent) state and solid film state were collected. The corresponding deprotected oligomers (through thermal annealing

treatment), i.e. HPBT and HTBT, were prepared as solid state film and in diluted DMF solution for UV/Vis spectroscopy experiments. The results of UV-Vis spectra were presented in Figure 2. For clarity, the spectra of mHocPBT and HPBT were arranged in Figure 2a and 2c, and the spectra of mHocTBT and HTBT were arranged in Figure 2b and 2d, respectively.

As for the soluble oligomers mHocPBT and mHocTBT, a bathochromic shift in the absorption onset point was observed from solution state to thin film state (Figure 2a and Figure 2b, black lines to red lines), which could be attributed to the packing of oligomer molecules in the solid states. Interestingly, mHocPBT and mHocTBT films show completely opposite changes in the UV/Vis absorption spectrum upon thermal deprotection (red lines to blue lines in Figure 2a and 2b). For mHocPBT film (Figure 2a), a large bathochromic shift of 53 nm on the absorption onset wavelength was observed after thermal annealing (forming HPBT film). The maximum absorption peak was bathochromically shifted for 48 nm as well. However, a 13 nm hypsochromic shift on the onset and 101 nm hypsochromic shift on the maximum absorption peak were observed (Figure 2b) for mHocTBT film via annealing (forming HTBT film).

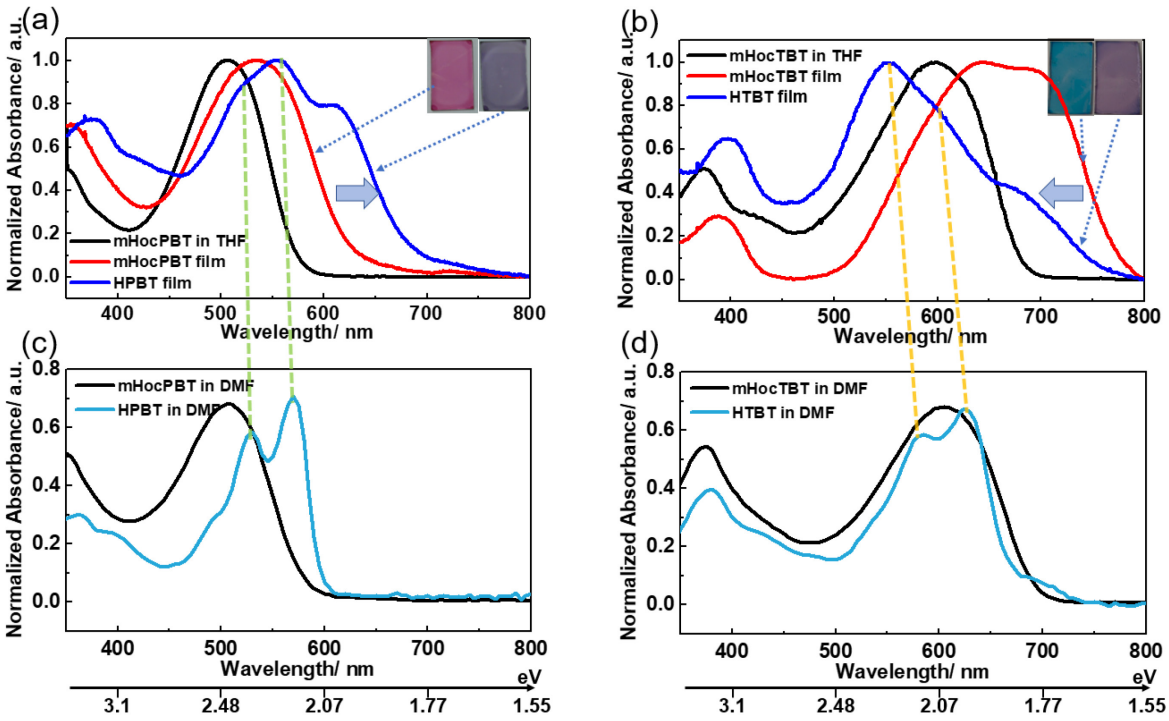

Figure 2. (a)Normalized UV/Vis absorption of spin-coated mHocPBT film and HPBT film (mHocPBT film thermal annealed at 200 °C for 5 min); (b) mHocTBT film and HTBT film; (c)mHocPBT and HPBT in DMF solution; (d)mHocTBT and HTBT in DMF solution.

Considering the electron-withdrawing nature of the mHoc group, the existence of mHoc promoted the intramolecular charge transfer (ICT) effects from the electron-donating thiophene units to electron-accepting central DPP core. Therefore, the elimination of side chains would weaken the ICT effects, which raises the lowest unoccupied molecular orbital energy levels (E_{LUMO}) and thus enlarge band gaps, causing hypsochromic shift [49, 63]. On the other hand, the removal of bulky mHoc group triggered the formation of intermolecular hydrogen-bonding networks and changed the intramolecular planarity of oligomer backbone [55], affecting the effective π-conjugation lengths and molecular stacking properties. In order to elucidate the UV/Vis spectra shifts in annealed solid films, the UV/Vis spectra of diluted solution containing original oligomers and

annealed oligomers were collected in Figure 2c and 2d. Since HPBT and HTBT have very poor solubility and were only slightly soluble in N, N-dimethylformamide (DMF), all the solution UV/Vis spectra in Figure 2c and 2d were measured in DMF solution. The assumption here was that the packing effect of the oligomer molecules was negligible in the diluted solution. From Figure 2c, the UV/Vis absorption maximum wavelength of HPBT was bathochromic shifted as compared with mHocPBT. As ICT effect (removing the electron-withdrawing side chain) causes hypsochromic shift, it was therefore clear that the intramolecular planarity (effective π-conjugation length) of HPBT must be significantly better than that of mHocPBT. In Figure 2d, the UV/Vis spectra of HTBT and mHocTBT was in a similar range, indicating that the collective effect of ICT and π-conjugation change was comparable before and after the removal of mHoc groups from mHocTBT. Because the removal of mHoc groups caused similar ICT effect for either mHocPBT or mHocTBT oligomers, it was expected that change of the effective π-conjugation length in PBT system (mHocPBT → HPBT, in diluted solution) was more dramatic than that in TBT system (mHocTBT → HTBT, in diluted solution) based on the observation in Figure 2c and 2d.

As for the solid oligomer film of HPBT and HTBT (as indicated in the Figure 2a and 2b, blue lines), significant packing induced absorption peak were observed in both systems as compared to their diluted solution states (Figure 2c and 2d, light blue lines). In HPBT film, the formation of intermolecular hydrogen bonding didn't change the original absorption peaks around 520 nm and 557 nm (indicated as green dash lines), suggesting a similar π-conjugation lengths in solid HPBT molecule (blue line in Figure 2a) and free HPBT molecule (in diluted solution, light blue line in Figure 2c). This can be ascribed as that the formation of intermolecular hydrogen bonding didn't cause significant conformation change of the HPBT molecules. In HTBT film, although a packing induced peak was still observed, the original absorption peaks (583 and 625 nm, light blue line in

Figure 2d) of free oligomers (in diluted DMF solution) were hypsochromically shifted to 556 nm and 599 nm (blue line in Figure 2b). The intensity of vibronic absorption peak at 556 nm (Figure 2b) increased dramatically and became the maximum absorption peak. This transition (indicated as orange dash lines) indicated that the intermolecular hydrogen bonding led to a possible conformational change of HTBT molecules [52, 64] in solid state. Even though, it was worth noting that significant packing effect was found in both systems and a lower band gap (higher onset absorption wavelength) was observed in annealed thin films as in diluted solution. The overall optical band gaps of TBT systems were smaller than corresponding molecules in PBT system. The optical band gaps calculated from the absorption onset for mHocPBT and mHocTBT films were 1.96 eV and 1.59 eV, which were changed to 1.79 eV and 1.61 eV after thermal deprotection. The detailed photophysical data are summarized in Table S2.To gain more insight of molecular structure change upon annealing, the single-crystal structures of mHocPBT and mHocTBT were investigated. The single crystals of both compounds were successfully grown by a vapor diffusion method, using chloroform and methanol as the good solvent and bad solvent, respectively. Table S2 summarized the basic parameters of the obtained single crystals and more details were available from the crystallography information files (CIFs) (SI). As shown in Figure 3, both molecules crystallized in the triclinic space group with a similar two dimensional lamellar packing in their unit cells. The π-π overlapping of both molecules also occurred in a similar way: one molecule was in parallel with adjacent molecules that were slipped by a length of one or two thiophene rings in the direction of the molecular backbone, as shown in Figure 3a and 3b. It is worth mentioning that the pi-stacking for mHocPBT was between the DPP core and the middle thiophene unit since the phenyl unit and the end thiophenyl unit were not parallel with the DPP core. However, the π-π stacking was between the DPP core and the end thiophenyl unit in the

mHocTBT molecules. The π-π stacking distance for mHocPBT and mHocTBT were 3.58 Å and 3.43 Å, respectively. The shorter π-π stacking distance indicated a tighter stacking of mHocTBT molecules than mHocPBT molecules. In fact, the UV/Vis spectrum of mHocTBT film showed a significant shoulder peak (red line in Figure 2b) and the UV/Vis spectrum of mHocPBT film didn't show obvious shoulder peak (red line in Figure 2a). The weaker π-π stacking in mHocPBT could be ascribed by its more distorted molecular conformation. The torsion angles of σ bonds between the conjugated rings of mHocPBT and mHocTBT molecules were shown in Figure 3c and 3d. The mHocTBT molecule had a quasi-coplanar conformation with all the three dihedral angles between the DPP core and adjacent thiophene rings less than 5°. For mHocPBT molecules, all the three dihedral angles were larger than 25°, suggesting a twisted molecular backbone and poor intramolecular coplanarity.

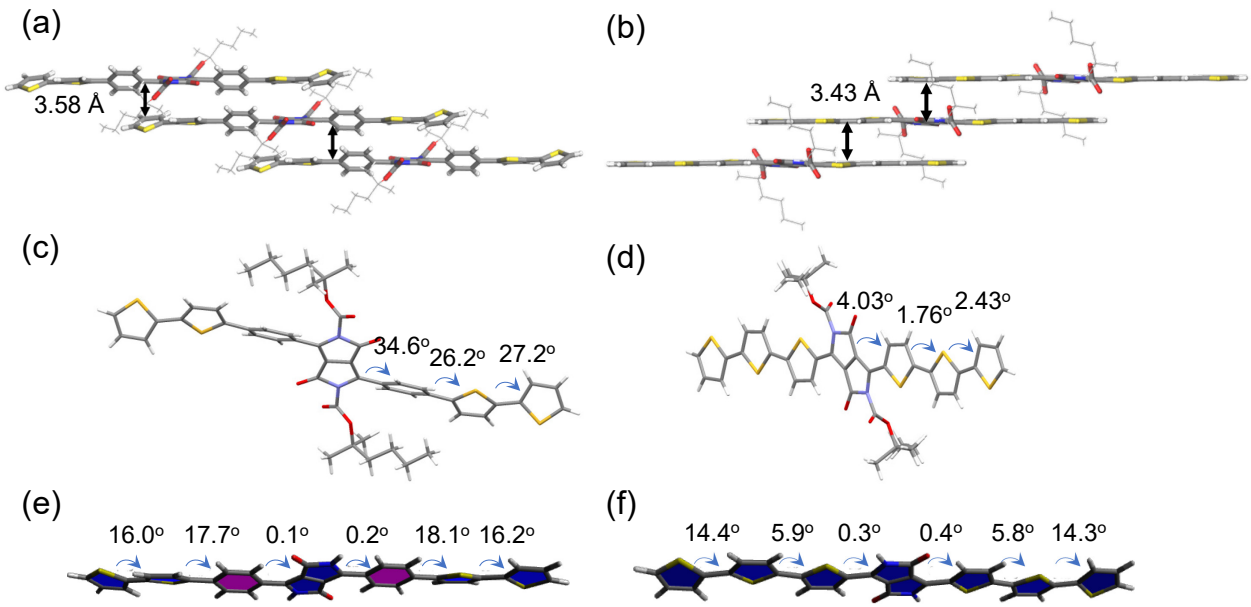

Figure 3. Crystal structure analysis of mHocPBT, mHocTBT, HPBT and HTBT. a) The packing structure of mHocPBT crystal. The π-π stacking (3.58 Å) is indicated in the figure. b) The packing structure of mHocTBT crystal. The π-π stacking (3.43 Å) is indicated in the figure. The molecular conformation of mHocPBT (c) and mHocTBT (d) with torsion angles between the aromatic units.

(e,f) Density functional theory (DFT) calculated the ground state geometry of HPBT and HTBT molecules. All torsion angles between aromatic rings are labeled in the figure.

After removing the mHoc group, HPBT and HTBT oligomers were obtained. However, both HPBT and HTBT had very poor solubility and were unable to form large crystal for single crystal X-ray diffraction experiments. Also the molecules of HPBT and HTBT were too large for physical vapor transport (PVT) and large crystals were not obtained even under reduce pressure PVT. Therefore, computational method [65-70] was employed to get more molecular conformation information of HPBT and HTBT. Although the computational study conducted here focused only on single oligomer molecule and the packing information was not included, it should reveal the conformation of the single molecule and could correlate with UV/Vis spectra in diluted solution to validate the intramolecular coplanarity. As shown in the density functional theory (DFT) calculated (see SI for the detailed method) ground state geometry (Figure 3e and 3f), both HPBT and HTBT exhibited very small torsion angles (less than 1^{o}) between DPP core and adjacent phenyl/thiophenyl rings. Therefore, by correlating the molecular conformation of both mHocPBT $\rightarrow$ HPBT (torsion angle from 34.6^{o} to 0.1~0.2^{o}) and mHocTBT $\rightarrow$ HTBT (torsion angle from 4.03^{o} to 0.3~0.4^{o}), it is clear that mHocPBT had a much larger enhancement of molecular conjugation efficiency than mHocTBT after they were converted to HPBT and HTBT, respectively. This results correlate very well with UV/Vis spectra in diluted solution (Figure 2c and 2d), where only PBT based oligomers exhibited significant bathochromic shift. As for the packing effect in the solid state, since both HPBT and HTBT molecules were planar in the free state (Figure 3e and 3f), it was expected to form π-π stacking structure in solid state. From the UV/Vis spectra of solid films, both HPBT and HTBT exhibited additional shoulder peak as compared with their dilute

solution spectra, suggesting a strong packing in solid state. However, the packing in solid state had different impact for the molecular conformation of HPBT and HTBT. Two maximum absorption peaks of HPBT in solution and HPBT in solid film overlapped well (green dash line in Figure 2), indicating similar molecular conformation in both states. That is, the intermolecular hydrogen bonding didn't change the molecular conformation of HPBT. On the contrary, two maximum absorption peaks of HTBT were blue-shifted in solid film as compared in diluted solution (orange dash lines in Figure 2), which could be explained by a more distorted molecular configuration of HTBT with the formation of intermolecular hydrogen bonding. Although lack of direct evidence like crystal structure of HTBT at solid state, it was expected that such an intermolecular hydrogen bonding might cause an increased torsion angles between DPP core and adjacent thiophene units in HTBT molecules at solid-state film.

One additional evidence of the formation of intermolecular hydrogen bonding after annealing was that the solubilities of HPBT and HTBT were very low, even though their precursor mHocPBT and mHocTBT had excellent solubility in organic solvent. The HPBT and HTBT films were solvent-resistant in THF, chloroform, dichloromethane, water and hexane. The solubilities of HPBT and HTBT films (formed by thermal annealing of mHocPBT and mHocTBT film) were quantitatively examined by measuring the film absorption before and after washing with solvents (Figure S4). The results showed that the intensity of absorption remained 98% and 95% after solvent washing for HPBT and HTBT films, respectively, suggesting the formation of strong hydrogen-bonded insoluble materials.

Cyclic voltammetry was performed to investigate the electrochemical properties of the mHocPBT and mHocTBT oligomers before and after thermal treatment. The oxidation and reduction onset potentials, highest occupied molecular orbital (HOMO) and lowest unoccupied molecular orbital

(LUMO) levels, electrochemical band gaps and the optical band gaps of non-annealed and annealed mHocPBT and mHocTBT were summarized in Table S3. As shown in Figure S5, both annealed films exhibited increased oxidation onset potential (thus increased HOMO levels) as compared with their pristine films. The reversibility of oxidation process was better in annealed films, which could be explained by the fact that the hydrogen-bonded annealed oligomers films had lower solubility in electrolyte solution. During the CV experiment of pristine films, a typical phenomenon was that the molecules became soluble at oxidative states due to the formation of charged molecules. As a result, the molecules could not stay on the ITO electrode and the reversibility of the CV cycles became poor. Both HPBT and HTBT exhibited a lower HOMO level than the corresponding soluble oligomers. However, the LUMO level of HPBT decreased but LUMO level of HTBT increased as compared with the corresponding soluble oligomers. As a result, the bandgap of HPBT decreased and bandgap of HTBT increased as compared with corresponding soluble oligomers. This results matched well with the optical bandgaps determined by UV/Vis spectra. It was worth to mention that the bandgap of HTBT was lower than that of HPBT, in both optical and electrochemical experiments.

Thin Film Structure and OFET Devices

To correlate the charge transport and film structure of oligomers, OFET devices of mHocPBT and mHocTBT were fabricated. They were evaluated before and after the mHoc group removal to investigate the influence of hydrogen-bonding formation on the charge transport properties. Bottom-gate/bottom-contact configuration was adopted with Si/SiO_2 (300 nm) as the gate electrode/dielectric layers and prepatterned gold as source and drain electrodes. The organic semiconductor solution was then spin-casted on the n-octadecyltrichlorosilane (OTS)-treated

substrates to complete the transistor fabrication. The device was annealed at 50 °C for an hour in argon before characterization. The as-prepared devices were measured in vacuum and then thermally annealed (Argon, 200°C for 30 min) for the second measurement. Figure 4a-4d illustrates the output and transfer characteristics of the pristine and annealed devices. For mHocPBT, no obvious FET behavior of the pristine film was observed. Even after the thermal annealing, the HPBT devices exhibited weak current and were unavailable to obtain a reliable transistor behavior due to the comparable leaking current from gate electrode. Thus only mHocTBT (Figure 4a and 4b) and HTBT (Figure 4c and 4d) devices are reported. The pristine mHocTBT film devices gave a hole mobility of 1.0×10^{-4} $cm^2/(V\cdot s)$ and on/off ratio of 5×10^3. The threshold voltage is 22 V. After thermal annealing, the HTBT device had an increased mobility of 1.4×10^{-3} $cm^2/(V\cdot s)$, with on/off ratio of 10^3 and the threshold voltage of -21 V.

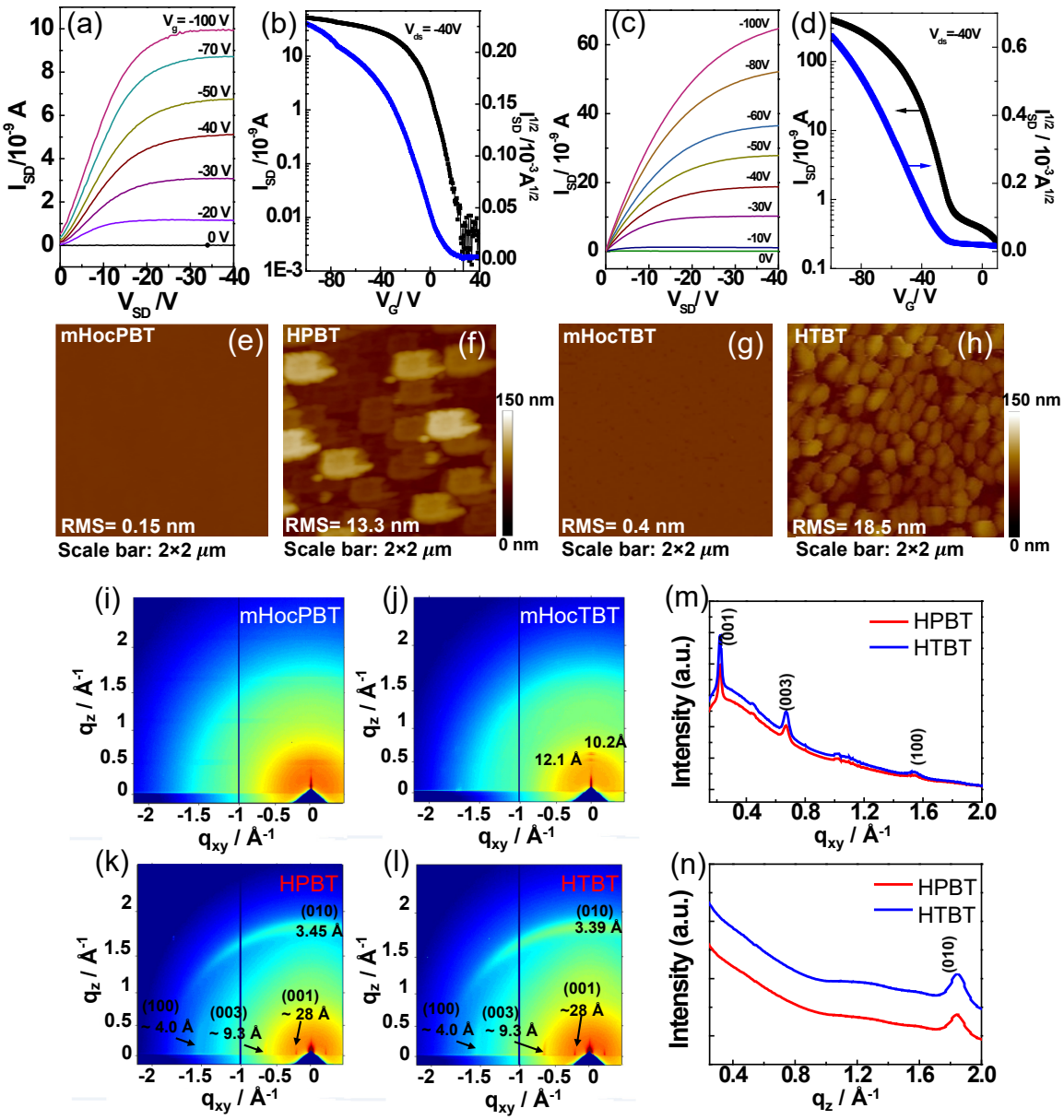

Figure 4. (a,b) The characteristic transfer and output curve of mHocTBT film device. (c,d) The characteristic transfer and output curve of HTBT film. (e-h) Tapping AFM images of mHocPBT (e), HPBT (f), mHocTBT (g) and HTBT (h). (i-l) 2D GIWAXS pattern of mHocPBT (i), mHocTBT (j), HPBT (k), and HTBT (l). (m,n) line-cut derived from (k) and (l) along q_{xy} and q_z direction, respectively.

To understand the charge transport in oligomer thin films, the microstructures of the as-casted and annealed mHocPBT and mHocTBT films were investigated. The surface topographic features and film crystallinity were examined by atomic force microscopy (AFM) and grazing incidence wide-angle X-ray scattering (GIWAXS) techniques. Figure 4e and 4f are AFM images of mHocPBT and HPBT films (after 30 min thermal annealing of same mHocPBT film sample), respectively. Figure 4g and 4h show the AFM images of mHocTBT and HTBT films, respectively. In both cases, the smooth spun-coated film became rougher, with root mean square (RMS) roughness increased from <1 nm to 10~20 nm. As compared with HPBT film, HTBT film consisted of more densely packed crystallites. The presence of large crystalline domains in these films proved the strong molecular aggregation within the annealed solid films, which should be contributed to the formation of hydrogen-bonding.

The GIWAXS patterns of these films are presented in Figure 4i-4l. There is no obvious diffraction peak identified for pristine mHocPBT film (Figure 4i). The lack of diffraction peak of as-casted mHocPBT films indicated that mHocPBT formed an amorphous film, which is absent of FET characteristics. By contrast, in Figure 4j, diffraction peaks at q_z = 0.62 Å^{-1} (d=10.2 Å), 0.52 Å^{-1} (d=12.1 Å) were observed for mHocTBT films, which attested to the fact that mHocTBT molecules formed active films with more ordered packing structure that delivered better FET characteristics than mHocPBT did. After thermal annealing, significant structure changes were observed on both films. In Figure 4k, 4l and 4n (corresponding 1D profile extracted along the q_z direction), the strong diffraction arcs at q_z =1.82 Å^{-1} (d=3.45 Å) and 1.85 Å^{-1} (d=3.39 Å) appeared for the HPBT and HTBT, respectively, which could be assigned as (010) diffraction relating to π-π stacking of the molecules. The relatively smaller d-spacing of the π-π stacking observed from the GIWAXS results than those extracted from the crystal data (3.58 Å and 3.43 Å for mHocPBT

and mHocTBT, respectively) could be interpreted as due to hydrogen-bonding mediated closer molecular stacking after mHoc groups were removed. Figure 4m shows the 1D profiles of HPBT and HTBT, extracted from Figure 4k and 4l along the q_{xy} direction. From figure 4k, 4l and 4m, three evident diffraction peaks at similar positions $q_{xy} \approx 0.22$ Å^{-1} (d ≈ 28.0 Å), 0.67 Å^{-1} (d ≈ 9.3 Å) and 1.57 Å^{-1} (d ≈ 4.0 Å) were observed for HPBT and HTBT. The first two peaks (d ≈ 28.0 Å and d ≈ 9.3 Å) with q ratio of 1:3 were indexed as (001) and (003) along the long-axis of conjugated molecules with d-spacing of ~ 28 Å, as shown in Figure S6. Similarly, diffraction peaks with d-spacing of ~ 4.0 Å along q_{xy} direction were indexed as (100), corresponding to molecular dimension along short-axis, as shown in Figure S6.[19] The (001), (003) and (100) diffractions along the q_{xy} direction and the π-π diffraction (010) in the q_z direction indicated that both hydrogen-bonded HPBT and HTBT molecules self-assembled into the face-on molecular orientation on the substrate. This could be explained by the fact that the face-on packing of oligomers avoids the direct contact of the polar hydrogen bonding sites to the hydrophobic OTS surface. Despite similar molecular orientation, the sharper (001), representing the higher crystallinity, and closer π-stacking contributed to the better mobility of HTBT-based devices over HPBT-based devices.

Conclusions

In summary, two DPP-based conjugated D-A oligomers mHocPBT and mHocTBT with latent hydrogen-bonding were synthesized in this work. The novel mHoc group render the oligomers with good solubility and able to be transferred to the hydrogen-bonded states by thermal annealing. Their structures and optical properties were characterized before and after the intermolecular hydrogen bonds were formed in the solid films. mHocTBT molecules exhibited a better coplanar structure than mHocPBT molecules. They also formed a closer π-π stacking structure in the solid state (mHocPBT ~ 3.58 Å and mHocTBT ~ 3.43 Å). Upon the removal of mHoc groups, the

intermolecular hydrogen-bonds were generated in the solid-state films. Without the intermolecular hydrogen-bonding, the free oligomer molecules (HPBT or HTBT) in diluted solution exhibited a similar planar conformation with center DPP units and adjacent aromatic units nearly at the same plane. As mHocPBT didn't have a coplanar conformation, the diluted solution of HPBT exhibited bathochromic shift as compared with mHocPBT. For oligomer mHocTBT, there was no obvious change on UV/Vis absorption since both mHocTBT and HTBT molecules had coplanar conformation. However, when the intermolecular hydrogen-bonding formed in HPBT and HTBT, which were true in their solid-state films, the coplanar molecular conformation of HPBT was kept but that of HTBT was distorted. Even though both HPBT and HTBT form pi-stacked structure, the maximum absorption wavelength of HTBT was hypsochromically shifted. As for the thin film structure, the spin-casted mHocPBT and mHocTBT didn't show visible crystal grain and HPBT and HTBT film formed by thermal annealing of corresponding soluble precursors' films showed large crystal grains. The molecular orientations of both HPBT and HTBT on the OTS treated surface were face-on. HTBT film exhibited an enhanced charge transport mobility than mHocTBT film due to a closer π-π stacking distance and a better crystalized structure, even though the oligomer HTBT was more distorted and had a large bandgap than mHocTBT in the solid state. This work indicated that the molecular conformation had large impact on the optical properties of the D-A oligomer semiconductor, however, the charge transport in the thin film was mainly governed by crystal grain size and π-π stacking.

Supplementary Information Available

Synthesis details of mHocPBT and mHocTBT, the properties of mHocPBT and mHocTBT including NMR spectrum, TGA information, crystallographic data, UV/Vis absorption of thermal

annealed oligomer films before and after solvent washing, properties of pristine and thermal annealed oligomer films including optical, electrochemical and molecular energy level data, cyclic voltammogram, DFT calculation method. This material is available free of charge via the Internet.

Conflicts of interest

The authors declare no competing financial interest.

Author contributions

[†]K.Y. and X.L. contributed equally to this work.

Acknowledgements

The authors thank the National Science Foundation (DMR-1554851) for financial support.

Notes and References

[1] S. R. Forrest and M. E. Thompson, *Chem. Rev.*, 2007, **107**, 923-925.

[2] T. B. Singh and N. S. Sariciftci, *Annu. Rev. Mater. Res.*, 2006, **36**, 199-230.

[3] A. C. Arias, J. D. MacKenzie, I. McCulloch, J. Rivnay and A. Salleo, *Chem. Rev.*, 2010, **110**, 3-24.

[4] A. D. Scaccabarozzi and N. Stingelin, *J. Mater. Chem. A*, 2014, **2**, 10818-10824.

[5] L. Torsi, M. Magliulo, K. Manoli and G. Palazzo, *Chem. Soc. Rev.*, 2013, **42**, 8612-8628.

[6] W. Zeng, L. Shu, Q. Li, S. Chen, F. Wang and X. M. Tao, *Adv. Mater.*, 2014, **26**, 5310-5336.

[7] T. Sekitani, H. Nakajima, H. Maeda, T. Fukushima, T. Aida, K. Hata and T. Someya, *Nat. Mater.*, 2009, **8**, 494-499.

[8] S. Günes, H. Neugebauer and N. S. Sariciftci, *Chem. Rev.*, 2007, **107**, 1324-1338.

[9] S. K. Hau, H. L. Yip and A. K. Y. Jen, *Polym. Rev.*, 2010, **50**, 474-510.

[10] L. Dou, Y. Liu, Z. Hong, G. Li and Y. Yang, *Chem. Rev.*, 2015, **115**, 12633-12665.

[11] K. Takimiya, Y. Kunugi and T. Otsubo, *Chem. lett.*, 2007, 36, 578-583.

[12] C. Wang, H. Dong, W. Hu, Y. Liu and D. Zhu, *Chem. Rev.*, 2011, **112**, 2208-2267.

[13] W. Wu, Y. Liu and D. Zhu, *Chem. Soc. Rev.*, 2010, **39**, 1489-1502.

[14] S. T. Bromley, M. Mas-Torrent, P. Hadley and C. Rovira, *J. Am. Chem. Soc.*, 2004, **126**, 6544-6545.

[15] Y. Diao, B. C. K. Tee, G. Giri, J. Xu, D. H. Kim, H. A. Becerril, R. M. Stoltenberg, T. H. Lee, G. Xue, S. C. B. Mannsfeld and Z. Bao, *Nat. Mater.*, 2013, **12**, 665-671.

[16] V. C. Sundar, J. Zaumseil, V. Podzorov, E. Menard, R. L. Willett, T. Someya, M. E. Gershenson and J. A. Rogers, *Science*, 2004, **303**, 1644−1646.

[17] J. Takeya, J. Kato, K. Hara, M. Yamagishi, R. Hirahara, K. Yamada, Y. Nakazawa, S. Ikehata, K. Tsukagoshi and Y. Aoyagi. *Phys. Rev. Lett*., 2007, **98**, No. 196804.

[18] O. D. Jurchescu, M. Popinciuc, B. J. van Wees and T. T. M. Palstra, *Adv. Mater.*, 2007, **19**, 688−692.

[19] J. Takeya, C. Goldmann, S. Haas, K. P. Pernstich, B. Ketterer and B. Batlogg, *J. Appl. Phys.*, 2003, **94**, 5800−5804.

[20] C. Goldmann, S. Haas, C. Krellner, K. P. Pernstich, D. J. Gundlach and B. Batlogg, *J. Appl. Phys.*, 2004, **96**, 2080−2086.

[21] C. Zhang, Y. Zang, E. Gann, C. R. McNeill, X. Zhu, C. A. Di and D. Zhu, *J. Am. Chem. Soc.*, 2014, **136**, 16176-16184.

[22] P. Gao, D. Beckmann, H. N. Tsao, X. Feng, V. Enkelmann, M. Baumgarten, W. Pisula and K. Müllen, *Adv. Mater.*, 2009, **21**, 213-216.

[23] Y. Zhang, C. Kim, J. Lin and T. Q. Nguyen, *Adv. Funct. Mater.*, 2012, **22**, 97−105.

[24] A. S. Molinari, H. Alves, Z. Chen, A. Facchetti and A. F. Morpurgo, *J. Am. Chem. Soc.*, 2009, **131**, 2462−2463.

[25] B. A. Jones, A. Facchetti, M. R. Wasielewski and T. J. Marks, *Adv. Funct. Mater.*, 2008, **18**, 1329−1339.

[26] B. A. Jones, M. J. Ahrens, M. H. Yoon, A. Facchetti, T. J. Marks and M. R. Wasielewski, *Angew. Chem. Int. Ed.*, 2004, **116**, 6523−6526.

[27] S. L. Suraru, U. Zschieschang, H. Klauk and F. Wü rthner, *Chem. Commun.*, 2011, **47**, 1767−1769.

[28] Y. Qiao, Y. Guo, C. Yu, F. Zhang, W. Xu, Y. Liu and D.Zhu, *J. Am. Chem. Soc.*, 2012, **134**, 4084− 4087.

[29] Y. Lin, P. Cheng, Y. Li and X. Zhan, *Chem. Commun.*, 2012, **48**, 4773−4775.

[30] T. He, M. Stolte and F. Würthner, *Adv. Mater.*, 2013, **25**, 6951− 6955.

[31] T. He, M. Stolte, C. Burschka, N. H. Hansen, T. Musiol, D. Kalblein, J. Pflaum, X. Tao, J. Brill and F. Würthner, *Nat. Commun.*, 2015, **6**, No. 5954.

[32] W. Yue, T. He, M. Stolte, M. Gsanger and F. Wü rthner, *Chem. Commun.*, 2014, **50**, 545−547.

[33] C. B. Nielsen, M. Turbiez and I. McCulloch, *Adv. Mater.*, 2013, **25**, 1859-1880.

[34] H. C. Zhang, S. Zhang, Y. F. Mao, K.W. Liu, Y. M. Chen, J. Zhang, J. Strzalka, W. J. Yang, C. L. Wange and Y. Zhu, *Polym. Chem*., 2017, **8**, 3255–3260.

[35] B. Tieke, A. R. Rabindranath, K. Zhang and Y. Zhu, *Beilstein J. Org. Chem.*, 2010, **6**, 830-845.

[36] Y. Zhu, K. Zhang and B. Tieke, *Macromol. Chem. Phys.*, 2009, **210**, 431-439.

[37] A. R. Rabindranath, Y. Zhu, K. Zhang and B. Tieke, *Polymer*, 2009, **50**, 1637-1644.

[38] Y. Zhu, A. R. Rabindranath, T. Beyerlein and B. Tieke, *Macromolecules,* 2007, **40**, 6981-6989.

[39] Y. Zhu, I. Heim and B. Tieke, *Macromol. Chem. Phys.*, 2006, **207**, 2206-2214.

[40] A. R. Rabindranath, Y. Zhu, I. Heim and B. Tieke, *Macromolecules*, 2006, **39**, 8250-8256.

[41] E. D. Glowacki, M. Irimia-Vladu, S. Bauer and N. S. Sariciftci, *J. Mater. Chem. B*, 2013, **1**, 3742-3753.

[42] K. Yang, T. He, X. Chen, S. Z. D. Cheng and Y. Zhu, *Macromolecules*, 2014, **47**, 8479-8486.

[43] F. Bruni, M. Sassi, M. Campione, U. Giovanella, R. Ruffo, S. Luzzati, F. Meinardi, L. Beverina and S. Brovelli, *Adv. Funct. Mater.*, 2014, **24**, 7410-7419.

[44] J. Lee, A. R. Han, J. Hong, J. H. Seo, J. H. Oh and C. Yang, *Adv. Funct. Mater.*, 2012, **22**, 4128-4138.

[45] E. D. Głowacki, M. Irimia-Vladu, M. Kaltenbrunner, J. Gsiorowski, M. S. White, U. Monkowius, G. Romanazzi, G. P. Suranna, P. Mastrorilli, T. Sekitani, S. Bauer, T. Someya, L. Torsi and N. S. Sariciftci, *Adv. Mater.*, 2013, **25**, 1563-1569.

[46] H. Yanagisawa, J. Mizuguchi, S. Aramaki and Y. Sakai, *Jpn. J. Appl. Phys.*, 2008, **47**, 4728-4731.

[47] T. Aytun, L. Barreda, A. Ruiz-Carretero, J. A. Lehrman and S. I. Stupp, *Chem. Mater.*, 2015, **27**, 1201-1209.

[48] B. Sun, W. Hong, H. Aziz and Y. Li, *J. Mater. Chem.*, 2012, **22**, 18950-18955.

[49] C. Liu, S. Dong, P. Cai, P. Liu, S. Liu, J. Chen, F. Liu, L. Ying, T. P. Russell, F. Huang and Y. Cao, *Acs. Appl. Mater. Inter.*, 2015, **7**, 9038-9051.

[50] H. Yanagisawa, J. Mizuguchi, S. Aramaki and Y. Sakai, *Jpn. J. Appl. Phys.*, 2008, **47**, No. 4728.

[51] E. D. Głowacki, H. Coskun, M. A. Blood-Forsythe, U. Monkowius, L. Leonat, M. Grzybowski, D. Gryko, M. S. White, A. Aspuru-Guzik and N. S. Sariciftci, *Org. Electron.*, 2014, **15**, 3521−3528.

[52] Y. Suna, J. I. Nishida, Y. Fujisaki and Y. Yamashita, *Org. Lett.*, 2012, **14**, 3356−3359.

[53] M. Irimia-Vladu, E. D. Głowacki, P. A. Troshin, G. Schwabegger, L. Leonat, D. K. Susarova, O. Krystal, M. Ullah, Y. Kanbur and M. A. Bodea, *Adv. Mater.*, 2012, **24**, 375−380.

[54] J. H. Oh, W.-Y. Lee, T. Noe, W.-C. Chen, M. Kö nemann and Z. Bao, *J. Am. Chem. Soc.*, 2011, **133**, 4204−4207.

[55] H. Zhang, R. Deng, J. Wang, X. Li, Y. Chen, K. Liu, C. J. Taubert, S. Z. D. Cheng and Y. Zhu, *ACS Appl. Mater. Interfaces,* 2017, **9**, 21891−21899.

[56] H. Zhang, K. Liu, K. Wu, Y. Chen, R. Deng, X. Li, H. Jin, S. Li, S. S. D. Chuang and Y. Zhu, *J. Phys. Chem. C*, 2018, **122**, 5888–5895

[57] M. Rooney, S. Mattiello, R. Stara, A. Sanzone, P. Brazzo, M. Sassi and L. Beverina, *Dyes and Pigments*, 2018, **149**, 893-901.

[58] Z. Hao and A. Iqbal, *Chem. Soc. Rev.*, 1997, **26**, 203-213.

[59] J. S. Zambounis, Z. Hao and A. Iqbal, *Nature*, 1997, **388**, 131–132.

[60] T. Naddo, Y. Che, W. Zhang, K. Balakrishnan, X. Yang, M. Yen, J. Zhao, J. S. Moore and L. Zang, *J. Am. Chem. Soc.*, 2007, **129**, 6978-6979.

[61] M. Kuhn, J. Ludwig, T. Marszalek, T. Adermann, W. Pisula, K. Müllen, A. Colsmann and M. Hamburger, *Chem. Mater.*, 2015, **27**, 2678-2686.

[62] D. J. Skrovanek, S. E. Howe, P. C. Painter and M. M. Coleman, *Macromolecules*, 1985, **18**, 1676-1683.

[63] H. Zhang, K. Yang, Y. Chen, R. Bhatta, M. Tsige, S. Z. D. Cheng and Y. Zhu, *Macromol. Chem. Phys.*, 2017, **218**, 1600617

[64] A. Mohebbi, J. Yuen, J. Fan, C. Munoz, M. Wang, R. S. Shirazi, J. Seifter and F. Wudl, *Adv. Mater.*, 2011, **23**, 4644–4648.

[65] P. Hohenberg and W. Kohn, *Phys. Rev.*, 1964, **136**, B864-B871.

[66] M. J. Frisch, et al. *Gaussian 09*, Revision D.01; Gaussian, Inc.: Wallingford, CT,2013.

[67] A. D. Becke, *J. Chem. Phys.*, 1993, **98**, 5648-5652.

[68] S. Grimme, *J. Comput. Chem.*, 2006, **27**, 1787-1799.

[69] R. S. Bhatta and M. Tsige, *ACS Appl. Mater. Interfaces*, 2014, **6**, 15889-15896.

[70] R. S. Bhatta and M. Tsige, *Polymer*, 2015, **56**, 293-299.